Building and Environment 248 (2024) 111083

Contents lists available at ScienceDirect

Building and Environment

journal homepage: www.elsevier.com/locate/buildenv

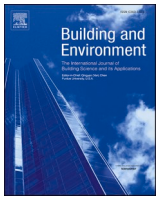

Closing the gap between traditional wind-driven rain studies and the performance-based design of building façades: Case study of the Netherlands

José M. Pérez-Bella [a,*], Javier Domínguez-Hernández [a], Pedro L. López-Julián [b], Ángel Salesa-Bordabana [b], Martín Orna-Carmona [b]

[a] Department of Construction Engineering, Engineering and Architecture School, University of Zaragoza, María de Luna, s/n, 50018, Zaragoza, Spain
[b] La Almunia Polytechnic University School, University of Zaragoza, c/ Mayor, 5, 50100 La Almunia de Doña Godina, Spain

ARTICLE INFO

Keywords:
Water tightness
Façade design
Climate loads
Test parameters
Performance assessment
Return period

ABSTRACT

Over the last few decades, analyses of wind-driven rain exposure on building façades have been conducted in multiple regions. Sometimes, these studies also included the driving rain wind pressure, thereby characterising both critical factors contributing to rainwater penetration into façade materials. However, practitioners typically rely on performance results obtained from standardised watertightness tests to make façade design decisions, even though these tests do not recreate the specific exposure combinations that can occur on each façade. Consequently, there is no quantitative correlation between the traditionally identified exposures and actual façade designs, resulting in pure qualitative choices and poorly optimised designs. This study addresses this issue by correcting the existing methodological deficiencies in a prior calculation procedure, which aims to relate the exposure parameters that the façade configuration withstood during any watertightness test to the expected climate exposures at its design operating conditions. New contributions are presented to enhance the method reliability as well as to reduce calculation effort and reliance on exhaustive weather data. The various climate parameters required to establish this relationship were analysed and tabulated for the Netherlands, enabling a truly performance-based design of façades to resist rainwater penetration throughout the country. Different methods of implementing this procedure, according to the availability of weather data, were also compared for façade case studies located in Amsterdam and Maastricht.

1. Introduction

Precipitation diverted by wind action, referred to as wind-driven rain (WDR), is the main source of water supply for building façades [1,2]. In conjunction with simultaneous wind pressure (driving rain wind pressure, DRWP), both contribute to rainwater runoff exceeding the thresholds of surface tension and the capillary pressure of water existing in the pores of construction materials, thus causing rainwater infiltration into façade materials [3–8]. This rainwater penetration, dependent on the façade features and climatic exposure, causes multiple issues concerning the thermal performance of the building envelope, premature deterioration of façades, and health complaints in building occupants (such as asthma and respiratory symptoms) [9–14].

Multiple studies have been developed to characterise wind-driven rain exposure throughout the world, mainly through semi-empirical approaches based on the so-called WDR relationship [15–19]. Occasionally, the analysis of wind pressure concurrent with WDR has complemented prior characterisation [20–22]. The utility of these traditional methods has been increased by progressively including more exhaustive weather records, directional analyses, calculation simplifications, and numerical methods based on computational fluid dynamics (for specific building configurations) [23–26].

However, all these exposures only result in generic regulatory requirements for façade designs (furthermore associated with wide exposure ranges), without providing specific watertightness guidelines for each case study. In turn, practitioners base their design decisions on the performance of façade configurations during standardised watertightness tests in which, for economy and functionality, the exposures expected in each case study are not recreated. In contrast, the façade samples are subjected to constant water supply and incremental pressure

* Corresponding author. Department of Construction Engineering, University of Zaragoza (UZ), María de Luna, s/n, 50018, Zaragoza, Spain.
E-mail address: jmpb@unizar.es (J.M. Pérez-Bella).

https://doi.org/10.1016/j.buildenv.2023.111083
Received 13 September 2023; Received in revised form 7 November 2023; Accepted 27 November 2023
Available online 1 December 2023

differences, whose generic values also differ among international tests [27–31]. Given that the standardised test parameters cannot be related to the extreme exposures expected for each façade, the watertightness performance of each façade design under actual operating conditions remains unknown. Thus, neither the traditional WDR studies support performance-based designs nor watertightness tests provide anything more than a purely qualitative approach for façade design.

To address this issue, a relationship between the standardised exposure parameters used in testing and the actual exposure conditions of any façade was proposed (Bayesian Performance-Based method, BPB method) [32]. This relationship is established by calculating the recurrence of tested parameters (i.e., return period) on any façade, considering its specific location, height, and surroundings. The method was subsequently extended to consider the influence of exposure durations recreated in watertightness tests on the return period calculation [33]. Finally, the calculation was modified to include accurate estimates of the wind profile under unstable atmospheric conditions and correct the WDR value associated with the diameter of the predominant raindrop [34]. However, the BPB method still has weaknesses that affect its accuracy and usefulness: *(i)* the difficulty of obtaining the required records of rainfall and wind speed associated with exhaustive recording intervals, and *(ii)* the uncertainty associated with the calculation of return periods based on wind speed records that do not consider their co-occurrence with rain events.

This study addresses both methodological weaknesses and provides a complete and functional database for the comprehensive implementation of the BPB method across the Netherlands. Section 2 compiles the foundations of the BPB method, which allows for the determination of the return period associated with the tested exposures for any façade case study. Section 3 presents new contributions that enhance the reliability of the method by considering the co-occurrence of rain and wind when calculating return periods, as well as its applicability by reducing the reliance on exhaustive weather records. A complete database for the functional implementation of the method in the Netherlands is also provided. Finally, Section 4 illustrates and discusses different approaches for implementing this comprehensive BPB method, considering the performance-based design of façades in two major Dutch cities: Amsterdam (located near the North Sea coast) and Maastricht (inland, near the borders with Belgium and Germany).

2. Background

The combination of two simultaneous climatic factors determines the risk of rainwater penetration into façade materials: the rainwater supply on the façade surface (i.e., WDR) and the wind pressure acting on this runoff (i.e., DRWP) [3,4,35]. Both factors are recreated during international watertightness tests by subjecting the exterior face of the façade sample to continuous water spray while applying static, cyclical or pulsating pressure differences [27–31].

Based on the watertightness performance of each façade configuration during the trial (water sprayed and maximum pressure difference withstood without penetration), the BPB method determines the recurrence of WDR and DRWP exposures equivalent to those surpassed during the test [32–34]. This recurrence is defined as a return period (in years), which depends on the test exposure surpassed (the higher its magnitude and duration, the greater the severity and corresponding return period), climatic conditions of the site, and façade features (height and surroundings), thus quantifying the façade performance under its designed operational conditions.

First, the DRWP exposure on the façade was estimated using the Bernoulli equation (Eq. 1), where $DRWP_z$ (Pa) represents the driving rain wind pressure at height z (m) of the façade and z_o (m) is the roughness length of the surrounding terrain, whose value is tabulated in the literature [36]. This roughness length is included in the Hellmann friction coefficient of the wind profile power law using an empirical formula suitable for unstable atmospheric conditions [37,38], such as those linked to the cloud formation mechanisms producing WDR events [39]. $U_{10\ sim}$ (m/s) represents the simultaneous wind speed record during precipitation, collected under reference conditions (open areas and at a height of 10 m above ground level for conventional meteorological records) [40]. For a conservative estimate, a pressure coefficient $C_p = 1$, constant air density $\rho = 1.2$ kg/m^3 and wind direction perpendicular to the façade orientation ($\cos\theta = 1$) can be used, thus simplifying Eq. (1) accordingly.

$$DRWP_z \approx C_p \cdot \frac{1}{2} \cdot \rho \cdot (U_{10\ \mathrm{sim}})^2 \cdot \left(\frac{z}{10}\right)^{2\cdot\left[0.18+0.13\cdot\log\ z_0+0.03\cdot(\log\ z_0)^2\right]} \cdot \cos\theta \tag{1}$$

Second, the façade WDR exposure was determined using Eq. (2), which combines a semi-empirical WDR relationship enhanced by 14 % to obtain a more realistic estimate of the phenomenon [41,42], a driving rain factor calculated using the inverse of the terminal falling speed of raindrops [43], and an estimate of the predominant spherical diameter of the droplets calculated from the rainfall records R_h (mm) [44]. Thus, WDR_z (mm) represents the wind-driven rain collected over the specified recording interval at façade height z (m) and $U_{10\ sim}$ (m/s) indicates the simultaneous wind speed with the adjustments mentioned in Eq. (1) [34]. The most unfavourable case is implicitly considered, corresponding to a wind direction perpendicular to the façade orientation. A rain admittance factor $RAF = 0.9$ can be applied to calculate the exposure at the uppermost corners of the building façade (the most unfavourable area).

$$WDR_Z \approx 1.14 \cdot RAF \cdot \frac{U_{10\ \mathrm{sim}} \cdot \left(\frac{z}{10}\right)^{\left[0.18+0.13\cdot\log\ z_0+0.03\cdot(\log\ z_0)^2\right]}}{-0.16603\cdot(R_h)^{-1}+4.92438\cdot(R_h)^{-0.768}-0.89002\cdot(R_h)^{-0.536}+0.05507\cdot(R_h)^{-0.304}} \tag{2}$$

To determine the *Return period* (years) associated with the probability of the simultaneous occurrence of WDR_{zi} and $DRWP_{zi}$ values, an approach to Bayes' theorem was proposed. Given that $DRWP_z$ depends only on the variable $U_{10\ sim}$ (see Eq. (1)), the occurrence probability of a specific $DRWP_{zi}$ value can be substituted by that of the linked $U_{10i\ sim}$ value (see Eq. (3)). In turn, the probability of WDR_{zi} exposure when the prior simultaneous wind speed $U_{10i\ sim}$ occurs can be expressed as the probability of the R_{hi} value that can be solved using Eq. (2). Thus, the BPB method transforms the mathematical problem into a straightforward probability calculation of the independent climate variables ($U_{10i\ sim}$ and R_{hi} values obtained from Eqs. (1) and (2), respectively).

$$\begin{aligned}\frac{1}{\text{Return period}\ (WDR_{Z\,i} \cap DRWP_{Z\,i})} &= P(WDR_{z\,i} \cap DRWP_{z\,i}) \\ &= P(DRWP_{z\,i}) \cdot P(WDR_{z\,i} | DRWP_{z\,i}) = P(U_{10i\ \mathrm{sim}}) \cdot P(R_{hi})\end{aligned} \tag{3}$$

To functionally calculate both independent probabilities, a Gumbel distribution (extreme value analysis) is recommended [34,45]. These probabilities $P(U_{10i\ sim})$ and $P(R_{hi})$ are determined by statistically analysing series of annual maxima relative to $U_{10\ sim}$ and R_h records, where $u_{(u10\ sim)}$ and $u_{(Rh)}$ represent the mode of both series and $\beta_{(u10\ sim)}$ and $\beta_{(Rh)}$ are the dispersion parameters. The formulations required to identify these parameters are listed in Table 1.

As a result, Eq. (4) completes the three-equation system that allows

Table 1
Scheme of the formulation used to calculate the Gumbel distribution parameters u and β from maximum annual records of rainfall and wind speed.

Symbol	*Formula*	*Magnitude description*
x_i	–	Maximum annual records of the analysed variable, linked to a specific recording interval
N	–	Number of input data x_i of the variable (years with maximum annual records).
x_{avg}	$x_{avg} = \frac{\sum x_i}{N}$	Data average of all the input data x_i.
σ_x	$\sigma_x = \sqrt{\frac{\sum (x_i - x_{avg})^2}{N}}$	Standard deviation of all the input data x_i.
y_i	$y_i = -\ln\left(\ln\left(\frac{N+1}{i}\right)\right)$	N values of the reduced variable y, ranging i from 1 to N.
y_{avg}	$y_{avg} = \frac{\sum y_i}{N}$	Data average of the N values of the reduced variable y_i..
σ_y	$\sigma_y = \sqrt{\frac{\sum (y_i - y_{avg})^2}{N}}$	Standard deviation of the N values of the reduced variable y_i.
$u_{(analysed\ variable)}$	$u = x_{avg} - u_y \frac{\sigma_x}{\sigma_y}$	Mode of the variable analysed (see Eq. (4)).
$\beta_{(analysed\ variable)}$	$\beta = \frac{\sigma_x}{\sigma_y}$	Dispersion parameter of the variable analysed (see Eq. (4)).

the determination of the return period associated with the occurrence of specific WDR_{zi} and $DRWP_{zi}$ exposures on any building façade. Knowing the façade features and location (i.e., $u_{(u10\ sim)}$, $u_{(Rh)}$, $\beta_{(u10\ sim)}$, $\beta_{(Rh)}$, z, and z_o values), the three-equation system (Eqs. (1), (2) and (4)) can be analytically solved by fixing two of the five unknowns: WDR_{zi}, $DRWP_{zi}$, *Return period*, $U_{10i\ sim}$ and R_{hi}.

$$\frac{1}{\text{Return period}\ (WDR_{Zi} \cap DRWP_{Zi})} \approx \left(1 - \exp^{-\exp^{\frac{u(U_{10\ sim}) - U_{10i\ sim}}{\beta(U_{10\ sim})}}}\right) \cdot \left(1 - \exp^{-\exp^{\frac{u(R_h) - R_{hi}}{\beta(R_h)}}}\right) \quad (4)$$

On one hand, the product of the water spray rate (mm/min) used in testing by the test duration (min) can be considered as the WDR_{zi} value (mm) and the pressure difference ΔP (Pa) surpassed by the façade configuration can be regarded as $DRWP_{zi}$. Accordingly, the $U_{10i\ sim}$ and R_{hi} values, as well as the return period associated with this combined exposure, can be determined. Thus, the watertightness performance of the façade configuration under actual conditions can be quantified by the return period associated with the maximum exposure it can withstand.

Furthermore, the $U_{10i\ sim}$ and R_{hi} values can be solved by fixing the water spray rate and duration established in the watertightness test (WDR_{zi} value) and setting a target *Return period* (years of watertightness to be achieved based on regulatory requirements and design decisions). This allows to obtain the pressure difference (i.e., the $DRWP_{zi}$ value) that must be overcome during the test to recreate the established return period. In this case, the equation system has two solutions: a combination of high $U_{10i\ sim}$ and low R_{hi}, and a combination of high R_{hi} ad low $U_{10i\ sim}$ (see Fig. 1). However, only the first solution is of interest, because it provides a higher $DRWP_{zi}$ value, which corresponds to a greater pressure difference to surpass in the watertightness test.

The other pairs of unknowns are not meaningful because $U_{10i\ sim}$ and R_{hi} are always intermediate variables and the water spray rate (WDR_{zi}) is a constant predetermined for each international watertightness test. Thus, solving the three-equation system quantifies the expected performance of building façades under their operating conditions (return period) or determines the test parameters to surpass to ensure the required design performance. Alternatively, it is also possible to compare the severity of different international watertightness tests for façades [33], indirectly enabling for potential enhancements of their testing parameters.

2.1. Weaknesses and limitations of the BPB method

However, this equation system presents conceptual and mathematical challenges:

- The exposure duration must be considered in the calculation of the return period; a longer duration of the same exposure corresponds to a lower probability of occurrence, indicating greater severity. Therefore, the exposures considered in Eqs. (1) and (2) are related to the specific duration recreated in each watertightness test (the differential pressure stages typically range from 5 to 15 min) [27–31]. Conversely, the available weather records at each location determine the recording interval used in Eq. (4), which defines the $u_{(u10\ sim)}$, $u_{(Rh)}$, $\beta_{(u10\ sim)}$, and $\beta_{(Rh)}$ values. When the test duration did not align with the available recording interval, an intermediate calculation was proposed to extrapolate the $U_{10i\ sim}$ and R_{hi} values obtained using Eqs. (1) and (2) to their equivalents in the recording interval required in Eq. (4) [33,34]. In this intermediate calculation, the available weather records of wind speed and rainfall were averaged or summed, respectively, to obtain aggregate recording intervals (e.g. 20-, 30-, and 40-min series based on 10-min records). Therefore, a series of maximum annual values associated with these additional intervals could also be produced. Using best-fit regressions that relate the average annual maxima of each interval, cross-multiplication could be used to extrapolate the equivalent extreme values of both variables across different recording intervals. However, this calculation

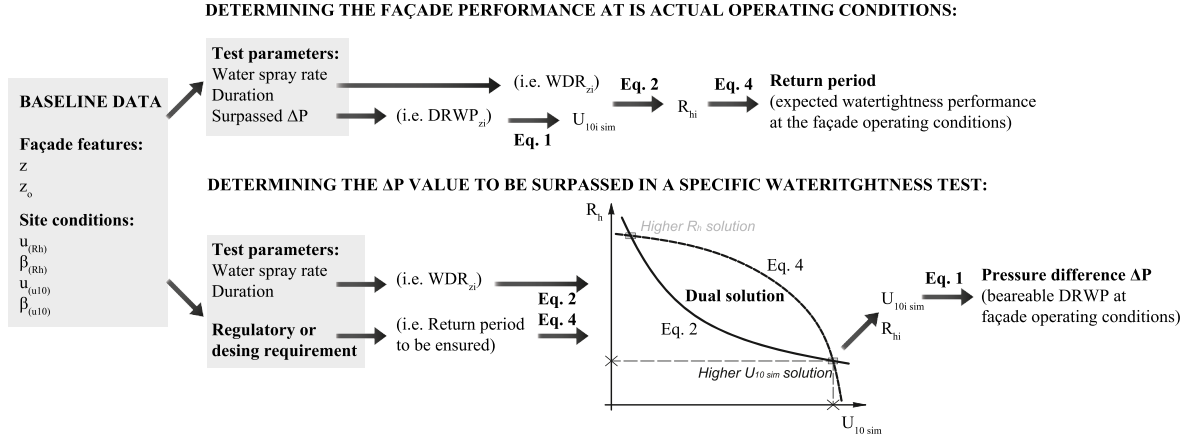

Fig. 1. Overview of the BPB method implementation.

is laborious and relies on the availability of exhaustive baseline records, thereby limiting the functionality and applicability of the BPB method in numerous locations with limited weather records.

- In turn, the summaries of the maximum annual wind speeds available at the locations do not usually account for their co-occurrence with rainfall. Consequently, only $u_{(u10)}$ and $\beta_{(u10)}$ values can be determined; thus, they may not be suitable for calculating the recurrence of wind speed values concurrent with precipitation such as those solved in Eq. (1). Similarly, the best-fit regressions mentioned in the previous paragraph do not account for wind records concurrent with rainfall, potentially affecting the reliability of the extrapolation across different recording intervals. Both factors introduce unknown uncertainties in the results of the BPB method.

The following section addresses these challenges by providing a comprehensive BPB method that is easily applicable everywhere (even with limited and non-concurrent rainfall and wind speed records), supporting façade design decisions in a performance-based and quantitative manner.

3. Method: A comprehensive implementation of the BPB method

To address the first limitation, a recent study developed a functional approach to accurately extrapolate extreme values of rainfall intensity (mm/min) and wind speed (m/s) across sub-daily recording intervals [46]. This approach uses a least-squares regression analysis (LSRA) to identify the best-fit regression that relates the average of the maximum annual values of both variables linked to different recording intervals [47]. The proposed general forms of these regressions were validated in over 100 locations primarily characterised by a temperate oceanic climate; however, the approach could be equally applicable to other climates [46].

For rainfall intensity, a potential-type regression was identified as the most suitable for relating extreme values associated with different sub-daily intervals (Eq. (5)) [46]. Thus, $R_{h\ (t)}$ (mm/min) represents the rainfall intensity associated with any specific t-minute recording interval during extreme precipitation events, whereas the empirical coefficients a and b adopt characteristic values at each location.

$$R_{h\ (t)} = a \cdot t^{-b} \tag{5}$$

Similarly, logarithmic regression was identified as the best method for relating extreme wind speeds associated with sub-daily intervals (Eq. (6)) [46]. In this case, $U_{\ 10(t)}$ (m/s) represents the extreme wind speed associated with a t-minute recording interval (without distinguishing concurrence with rainfall) and c and d are empirical coefficients that also adopt characteristic values at each location.

$$U_{10(t)} = -c \cdot \ln(t) + d \tag{6}$$

In practice, the potential and logarithmic regressions can be identified based on the summaries of the maximum annual records belonging to only two sub-daily recording intervals, applying a LSRA to their averages (e.g. hourly and daily records, to mention the most common ones). Common spreadsheets can be used for LSRA implementation, thus determining the empirical coefficients a, b, c and d. As a result, Eq. (5) can be directly included in the BPB method to functionally extrapolate the R_{hi} value obtained in Eq. (2) to any other required recording interval in Eq. (4) using cross-multiplication.

However, the application of the logarithmic regression can decrease the reliability of the BPB method because it does not consider wind records that are specifically simultaneous with precipitation. This issue requires to address the uncertainty associated with the methodological weakness mentioned in the second place. For this purpose, a general form of regression between extreme wind speeds and those that occur simultaneously with rainfall can be proposed. This general regression would enable the extrapolation of any extreme value concurrent with precipitation $U_{10i\ sim}$ to its equivalent speed value U_{10i} not concurrent with the rainfall. This approach would considerably decrease the calculation effort required by the BPB method, while enhancing its accuracy and applicability in locations with limited and non-concurrent rainfall and wind speed records: the extrapolated U_{10i} value could be directly used in Eq. (6) to calculate the equivalent U_{10i} value associated with any other required recording interval in Eq. (4) through cross-multiplication. The resultant value could also be directly applied to Eq. (4) using $u_{(u10)}$ and $\beta_{(u10)}$ values that were not obtained from records concurrent with rainfall.

The implementation of these methodological improvements was exemplified and validated in the Netherlands, enabling the comprehensive application of the BPB method, even with limited and non-simultaneous weather records. For this purpose, empirical coefficients, correlations, and mode and dispersion parameters applicable to locations distributed throughout the country are provided.

3.1. Performance-based design of building façades against rainwater penetration in the Netherlands

To ensure comprehensive implementation of the BPB method in the Netherlands, this study analysed simultaneous hourly records from 28 Dutch weather stations collected over a ten-year period (2010–2019) (see Fig. 2). In the case of wind speed, the hourly records were completed with gust records (3-s intervals) corresponding to each hourly interval. All data were collected by The Royal Netherlands Meteorological Institute, in accordance with the requirements set by the World Meteorological Organization (WMO) [40,48]. Stations with more than 10 % missing data or without weather records in any of the ten years considered were excluded to ensure the representativeness of the results. On average, 7.7 % of the data were missing, ranging from 3.1 % at the Arcen and Hoek Van Holland stations to 9.9 % at Hoorn (Terschelling).

All the analysed locations have a temperate oceanic climate because of their proximity to the Atlantic Ocean and are subject to occasional extratropical cyclones (low-pressure areas) that are more frequent and intense in winter [49,50]. Their altitudes range between −4.3 m (Rotterdam) and 114.3 m (Maastricht), as a result of the flat topography of the country. The lack of significant mountain ranges contributes to the maintenance of relatively uniform average annual rainfall and wind speeds across the country, which only increase near the coast. The mean annual rainfall ranges from 652 mm/yr (Ell) to 890 mm/yr (Rotterdam). In turn, the average wind speed ranges between 3.0 m/s (Arcen and Heino stations) and 7.0 m/s (Hoek Van Holland).

Additional data series of rainfall and wind speed, corresponding to other recording intervals (6, 8, 12, and 24 h), were produced by applying the aggregation and averaging procedures established by the WMO based on the available hourly records [40]. Rainfall intensity $R_{h\ (t)}$ was expressed in typical units for wind-driven rain calculations (mm/min; see Eq. (5)). The accumulated rainfall (mm) was divided by the duration t (min) of each recording interval. The wind speed records $U_{10(t)}$ were expressed in m/s for each recording interval (see Eq. (6)). Thus, the annual maxima of both variables linked to different recording intervals can be determined and subsequently averaged to identify a single representative value per variable, recording interval, and location. For wind speed, the maximum annual gust records were also included. Consequently, the site-specific potential and logarithmic regressions that best correlated these averages (Eqs. (5) and (6)) were identified by determining the most suitable coefficients a, b, c, and d using a LSRA (Table 2).

Furthermore, the series of wind speed data were re-elaborated by discarding wind records that did not occur simultaneously with precipitation. The resultant series allowed the maximum annual values of wind speed concurrent with rainfall linked to each recording interval (gust, 1, 6, 8, 12 and 24 h) to be obtained and average them to obtain a single representative value per recording interval and location. This re-analysis had the following objectives:

#	Location	Longitude (DD)	Latitude (DD)	Altitude (m)
1	De Kooy airfield	4.781	52.928	1.2
2	Amsterdam - Schiphol	4.790	52.318	-3.3
3	Berkhout	4.979	52.644	-2.4
4	Hoorn (Terschelling)	5.346	53.392	0.7
5	De Bilt	5.180	52.100	1.9
6	Stavoren	5.384	52.898	-1.3
7	Lelystad	5.520	52.458	-3.7
8	Marknesse	5.888	52.703	-3.3
9	Deelen	5.873	52.056	48.2
10	Lauwersoog	6.200	53.413	2.9
11	Heino	6.259	52.435	3.6
12	Hoogeveen	6.574	52.750	15.8
13	Eelde	6.585	53.125	5.2
14	Hupsel	6.657	52.069	29.1
15	Nieuw Beerta	7.150	53.196	-0.2
16	Twenthe	6.891	52.274	34.8
17	Vlissingen	3.596	51.442	8
18	Westdorpe	3.861	51.226	1.7
19	Hoek Van Holland	4.122	51.992	11.9
20	Rotterdam	4.447	51.962	-4.3
21	Cabauw	4.926	51.970	-0.7
22	Gilze-Rijen	4.936	51.566	14.9
23	Herwijnen	5.146	51.859	0.7
24	Eindhoven	5.377	51.451	20.6
25	Volkel	5.707	51.659	22
26	Ell	5.763	51.198	30
27	Maastricht	5.762	50.906	114.3
28	Arcen	6.197	51.498	19.5

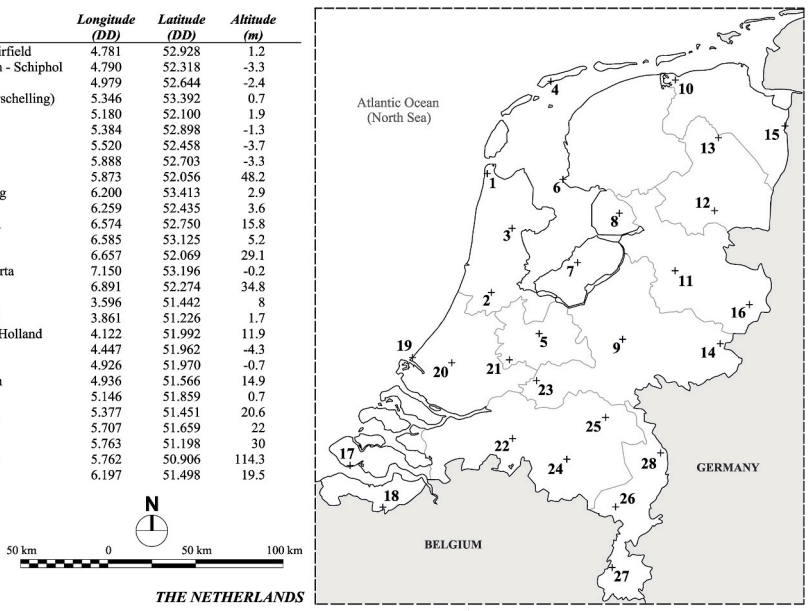

Fig. 2. Geographic distribution of the weather stations analysed.

Table 2
Summary of the empirical coefficients *a* and *b* used for the regression of extreme rainfall intensities between different recording intervals (Eq. (5)) as well as the *c* and *d* coefficients associated with wind speed extremes (Eq. (6)).

Location	Regression of extreme rainfall intensity (Eq. (5))			Regression of extreme wind speed (Eq. (6))		
	a	b	R^2	c	d	R^2
De Kooy airfield	3.402	0.686	*0.998*	1.502	25.565	*0.995*
Amsterdam - Schiphol	3.521	0.638	*0.997*	1.346	23.830	*0.996*
Berkhout	5.114	0.724	*0.998*	1.484	24.431	*0.997*
Hoorn (Terschelling)	5.745	0.771	*0.998*	1.422	26.381	*0.995*
De Bilt	6.663	0.738	*0.999*	1.614	20.377	*0.988*
Stavoren	4.832	0.751	*0.999*	1.419	24.815	*0.997*
Lelystad	7.035	0.794	*1.000*	1.564	23.646	*0.998*
Marknesse	6.666	0.770	*0.996*	1.436	21.231	*0.998*
Deelen	9.625	0.778	*0.999*	1.670	21.942	*0.994*
Lauwersoog	5.844	0.767	*1.000*	1.355	26.567	*0.995*
Heino	5.865	0.758	*0.999*	1.534	20.013	*0.996*
Hoogeveen	6.222	0.768	*0.998*	1.417	21.028	*0.996*
Eelde	4.485	0.741	*0.998*	1.449	22.144	*0.997*
Hupsel	5.779	0.729	*0.994*	1.596	20.999	*0.998*
Nieuw Beerta	6.896	0.777	*0.998*	1.344	23.010	*0.997*
Twenthe	7.623	0.772	*1.000*	1.540	20.455	*0.998*
Vlissingen	4.042	0.688	*0.999*	1.456	27.302	*0.994*
Westdorpe	3.429	0.671	*0.999*	1.632	23.420	*0.998*
Hoek Van Holland	6.535	0.758	*0.999*	1.470	27.828	*0.992*
Rotterdam	3.874	0.687	*0.999*	1.533	23.080	*0.994*
Cabauw	7.376	0.768	*0.999*	1.487	23.871	*0.997*
Gilze-Rijen	6.832	0.761	*1.000*	1.503	20.624	*0.997*
Herwijnen	8.853	0.780	*0.998*	1.450	22.417	*0.999*
Eindhoven	5.588	0.754	*0.997*	1.676	22.228	*0.998*
Volkel	7.534	0.787	*0.997*	1.651	22.446	*0.996*
Ell	5.324	0.753	*0.998*	1.603	22.143	*0.996*
Maastricht	9.401	0.804	*1.000*	1.503	22.059	*0.996*
Arcen	5.526	0.729	*0.996*	1.538	19.657	*0.998*
Average correlation			***0.998***			***0.996***

Table 3
Summary of empirical coefficients c_{sim} and d_{sim} applicable in Eq. (6) for the regression of extreme records of wind speed simultaneous to rainfall.

Location	Regression of extreme wind speed CONCURRENT with rainfall (Eq. (6))		
	c_{sim}	d_{sim}	R^2
De Kooy airfield	1.919	23.763	*0.958*
Amsterdam - Schiphol	1.756	22.200	*0.937*
Berkhout	1.846	22.918	*0.952*
Hoorn (Terschelling)	1.802	24.508	*0.925*
De Bilt	1.784	18.856	*0.996*
Stavoren	1.867	23.874	*0.945*
Lelystad	1.872	22.201	*0.966*
Marknesse	1.721	19.783	*0.974*
Deelen	1.828	20.405	*0.991*
Lauwersoog	1.861	25.367	*0.940*
Heino	1.759	18.814	*0.989*
Hoogeveen	1.700	20.209	*0.984*
Eelde	1.799	21.208	*0.977*
Hupsel	1.866	20.116	*0.991*
Nieuw Beerta	1.703	21.744	*0.953*
Twenthe	1.674	19.025	*0.990*
Vlissingen	2.037	25.464	*0.949*
Westdorpe	1.933	21.562	*0.983*
Hoek Van Holland	1.816	25.997	*0.936*
Rotterdam	1.913	21.666	*0.982*
Cabauw	1.922	22.506	*0.981*
Gilze-Rijen	1.810	19.519	*0.987*
Herwijnen	1.859	21.362	*0.974*
Eindhoven	1.927	21.028	*0.992*
Volkel	2.034	21.940	*0.990*
Ell	1.760	20.166	*0.987*
Maastricht	1.973	21.394	*0.963*
Arcen	1.729	18.566	*0.994*
Average correlation			***0.971***

- The mode and dispersion parameters required to solve Eq. (4) can be directly calculated based on this re-elaborated series of screened wind speed data concurrent with rainfall, ensuring an appropriate calculation of the return period. Thus, $u_{(u10\ sim)}$ and $\beta_{(u10\ sim)}$ values that were specifically suitable for wind speed extremes concurrent with rainfall are identified for each recording interval and location.
- The average of these re-elaborated annual wind speed maxima was related across different recording intervals by means using the LSRA. The results demonstrate that Eq. (6) can be equally applied for extreme wind speed records concurrent with rainfall. The average coefficient of determination R^2 was 0.971 at the 28 Dutch locations (the closer the coefficient is to 1, the better the data correlation). The LSRA performed for this validation also provided analogous

empirical coefficients c_{sim} and d_{sim} for application to Eq. (6), thereby improving the accuracy of the logarithmic regression (Table 3).

- The average of annual wind speed maxima concurrent with rainfall could be also compared with their equivalents based on all available wind records (without any distinction) for identical recording intervals. A strong correlation was found between both groups of average maxima in the 28 Dutch locations analysed, defined by a general form of linear regression (Eq. (7)). U_{10} (m/s) represents the conventional value of extreme wind speed, whereas $U_{10\ sim}$ (m/s) is the equivalent wind speed concurrent with rainfall.

$$U_{10} = e \cdot U_{10\ sim} + f \tag{7}$$

The empirical site-specific coefficients e and f that define this linear regression, derived from records associated with all analysed recording intervals (i.e., gust, 1, 6, 8, 12, and 24 h), are tabulated in Table 4. In practice, this linear regression can also be identified based on only two sub-daily recording intervals, resulting in a reduced calculation effort for extrapolation. The extrapolated U_{10i} values can be directly used in Eq. (4), in combination with conventional $u_{(u10)}$ and $\beta_{(u10)}$ values that do not consider the simultaneous occurrence of rainfall, allowing for the calculation of return periods even at sites with limited climate records.

The average coefficient of determination for the regressions of these sites is 0.973. These high coefficients of determination, as well as the homogeneous conditions throughout the Netherlands, indicate the potential for establishing a general linear regression applicable to the entire country. For this purpose, the maximum annual wind speed values of the 28 locations relative to each recording interval were averaged (see Supplementary material). Thus, the sole representative values for concurrent and non-concurrent records linked to each recording interval were determined (see black dots in Fig. 3). Subsequently, the general coefficients e and f applicable throughout the country were identified using the LSRA (Eq. (8)).

Table 4
Summary of the linear regression coefficients e and f identified between extreme wind speeds concurrent and non-concurrent with precipitation at each location (Eq. (7)). Those generically proposed for the Dutch territory are also shown (Eq. (8)).

Location	Regression between extreme U_{10} and $U_{10\ sim}$ values (Eq. (7))		
	E	f	R^2
De Kooy airfield	0.755	7.382	*0.969*
Amsterdam - Schiphol	0.725	7.408	*0.949*
Berkhout	0.768	6.528	*0.957*
Hoorn (Terschelling)	0.739	7.860	*0.944*
De Bilt	0.899	3.378	*0.979*
Stavoren	0.725	7.212	*0.960*
Lelystad	0.812	5.420	*0.976*
Marknesse	0.812	5.082	*0.970*
Deelen	0.906	3.392	*0.986*
Lauwersoog	0.690	8.749	*0.949*
Heino	0.860	3.734	*0.980*
Hoogeveen	0.819	4.371	*0.977*
Eelde	0.790	5.270	*0.981*
Hupsel	0.846	3.906	*0.984*
Nieuw Beerta	0.758	6.294	*0.963*
Twenthe	0.909	3.079	*0.985*
Vlissingen	0.688	9.535	*0.971*
Westdorpe	0.829	5.417	*0.979*
Hoek Van Holland	0.775	7.403	*0.970*
Rotterdam	0.784	5.951	*0.968*
Cabauw	0.757	6.693	*0.972*
Gilze-Rijen	0.820	4.536	*0.985*
Herwijnen	0.762	5.988	*0.979*
Eindhoven	0.860	4.064	*0.985*
Volkel	0.799	4.803	*0.975*
Ell	0.903	3.870	*0.993*
Maastricht	0.737	6.074	*0.967*
Arcen	0.885	3.194	*0.992*
Average correlation			***0.973***
General linear regression for the Netherlands (Eq. (8)):			
	0.800	**5.500**	***0.975***

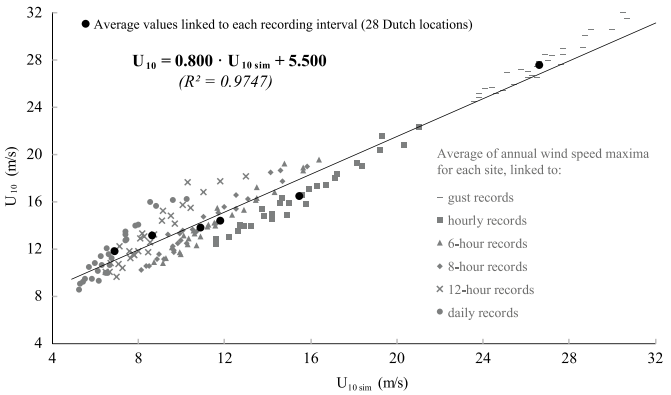

Fig. 3. General linear regression between annual wind speed maxima concurrent and non-concurrent with rainfall throughout the Netherlands.

$$U_{10} = 0.800 \cdot U_{10\ sim} + 5.500 \tag{8}$$

A complete list of the aforementioned averages of the annual maxima, as well as the mode and dispersion parameters for analysed recording intervals is available in the Supplementary material. As exemplified in the following section, this database allows the accurate implementation of the BPB method in a functional and comprehensive manner throughout the Netherlands, even at locations with limited weather records.

4. Implementation examples and discussion

The proposed implementation of the BPB method is illustrated in two major Dutch cities characterised by slightly different environmental conditions (despite the homogeneity of the country): Amsterdam (airport Schiphol, near the North Sea coast) and Maastricht (inland). Two hypothetical building façades with differentiated features were analysed by applying both resolution options available in the BPB method (i.e., characterising the façade performance at its operating conditions and determining the ΔP to be surpassed in a particular watertightness test).

In the case of Amsterdam, the aim was to quantify the watertightness performance of a building façade of 9 m height located on the capital's outskirts. For the purpose of analysis, it is assumed that the façade configuration withstood a pressure difference ΔP equal to 300 Pa during the EN 12865 watertightness test, which is characterised by 10-min pressure stages and a water spray rate of 2 mm/min [27]. In the case of Maastricht, the intended design was a curtain wall with a height of 26 m in the centre of the city, capable of providing 50 years of watertightness. For this, the minimum pressure difference ΔP to be overcome during the EN 12155 test (characterised by 5-min pressure stages and a water spray rate of 2 mm/min) was determined [51,52]. Although European tests were selected for both examples (coherent with the locations analysed), it is also possible to use any other international watertightness test by simply applying its specific duration and water spray rate.

4.1. Implementation of the comprehensive BPB method using the database provided

The comprehensive BPB method was applied using all data series and recording intervals produced from the available hourly data. The calculation parameters associated with both locations (site conditions) and features of the façades are summarised in Table 5 (extracted from the Supplementary material). For the calculation, the mode and

Table 5
Summary of the calculation parameters applicable in the two locations and features of the two façades analysed (height and surroundings).

	AMSTERDAM					
Altitude (m)	Longitude (DD)		Latitude (DD)		Average rainfall (mm/yr)	Average wind speed (m/s)
−3.3	4.790		52.318		821	4.9
Façade features:						
Height (m):	9.0	**Roughness length z_0 (m):**		1.5 (city outskirts) [34]		
Site conditions:						
Maximum rainfall intensity (mm/min); Average of maximum annual records for each recording interval:						
	60' (hour)	**360′**	**480′**	**720′**	**1440' (day)**	Eq. (5) (Table 2)
	0.257	0.085	0.065	0.056	0.033	$\Rightarrow R_{h\,(t)} = 3.521 \cdot t^{-0.638}$
$u_{(Rh)}$:	12.984				*(Potential-type regression by LSRA)*	
$\beta_{(Rh)}$:	4.859					
Maximum wind speed CONCURRENT with rainfall (m/s); Average of maximum annual records for each recording interval:						
3" (gust)	**60' (hour)**	**360′**	**480′**	**720′**	**1440' (day)**	Eq. (6) (Table 3)
26.600	17.200	13.483	11.988	9.125	7.383	$\Rightarrow U_{10(t)} = -1.756 \cdot \ln(t) + 22.200$
$u_{(u10\ sim)}$:	16.189				*(Logarithmic-type regression by LSRA)*	
$\beta_{(u10\ sim)}$:	2.042					

	MAASTRICHT					
Altitude (m)	**Longitude (DD)**		**Latitude (DD)**		**Average rainfall (mm/yr)**	**Average wind speed (m/s)**
114.3	5.762		50.906		726	3.9
Façade features:						
Height (m):	26.0	**Roughness length z_0 (m):**		3.0 (downtown city area with high rise buildings) [34]		
Site conditions:						
Maximum rainfall intensity (mm/min); Average of maximum annual records for each recording interval:						
	60' (hour)	**360′**	**480′**	**720′**	**1440' (day)**	Eq. (5) (Table 2)
	0.350	0.084	0.065	0.047	0.027	$\Rightarrow R_{h\,(t)} = 9.401 \cdot t^{-0.804}$
$u_{(Rh)}$:	13.767				*(Potential-type regression by LSRA)*	
$\beta_{(Rh)}$:	14.586					
Maximum wind speed CONCURRENT with rainfall (m/s); Average of maximum annual records for each recording interval:						
3" (gust)	**60' (hour)**	**360′**	**480′**	**720′**	**1440' (day)**	Eq. (6) (Table 3)
26.500	15.800	10.567	9.375	7.117	5.717	$\Rightarrow U_{10(t)} = -1.973 \cdot \ln(t) + 21.394$
$u_{(u10\ sim)}$:	14.639				*(Logarithmic-type regression by LSRA)*	
$\beta_{(u10\ sim)}$:	2.345					

dispersion parameters corresponding to the closest available recording interval to the typical duration of the watertightness tests were considered (i.e., hourly parameters).

To determine the expected watertightness performance of the façade in Amsterdam, the wind speed required to produce a DRWP exposure of 300 Pa on the analysed façade can be obtained by solving Eq. (1).

$$300\ \text{Pa} = 1 \cdot \frac{1}{2} \cdot 1.2 \cdot \left(U_{10\ \text{sim}(10\ \text{min})}\right)^2 \cdot \left(\frac{9}{10}\right)^{2 \cdot \left[0.18 + 0.13 \cdot \log\ 1.5 + 0.03 \cdot (\log\ 1.5)^2\right]} \cdot 1$$

$$U_{10\ \text{sim}(10\ \text{min})} = 22.846\ \text{m/s}$$

In turn, the rainfall intensity required to produce 20 mm of WDR exposure on this particular façade (2 mm/min applied over 10 min), with a concurrent wind speed of 22.846 m/s, can be obtained using Eq. (2):

$$20\ mm = 1.14 \cdot 0.9 \cdot \frac{22.846 \cdot \left(\frac{9}{10}\right)^{\left[0.18 + 0.13 \cdot \log\ 1.5 + 0.03 \cdot (\log\ 1.5)^2\right]}}{-0.16603 \cdot \left(R_{h(10\ \text{min})}\right)^{-1} + 4.92438 \cdot \left(R_{h(10\ \text{min})}\right)^{-0.768} - 0.89002 \cdot \left(R_{h(10\ \text{min})}\right)^{-0.536} + 0.05507 \cdot \left(R_{h(10\ \text{min})}\right)^{-0.304}}$$

$$R_{h\ (10\ \text{min})} = 4.522\ \text{mm} = 0.452\ \text{mm/min}$$

To replace both 10-min values in Eq. (4) (where the u and β values correspond to the hourly recording interval available at the location), it is necessary to apply cross-multiplication based on Eqs. (5) and (6). Thus, the hourly values equivalent to both 10-min variables can be obtained as follows:

$$R_{h\ (60\ \text{min})} = R_{h(10\ \text{min})} \cdot \frac{3.521 \cdot 60^{-0.638}}{3.521 \cdot 10^{-0.638}} = 0.144\ \text{mm/min} = 8.64\ \text{mm}$$

$$U_{10\ \text{sim}(60\ \text{min})} = U_{10\ \text{sim}(10\ \text{min})} \cdot \frac{-1.756 \cdot \ln(60) + 22.200}{-1.756 \cdot \ln(10) + 22.200} = 18.887\ \text{m/s}$$

The resulting hourly values were substituted into Eq. (4) to determine the return period associated with the maximum exposure that this façade configuration could withstand at its design operating conditions (Amsterdam, 9 m height, outskirts of the city). To increase the calculation accuracy, the mode and dispersion parameters corresponding to the maximum annual wind speeds during rainfall were used in Eq. (4) (i.e., $u_{(u10\ sim)}$ and $\beta_{(u10\ sim)}$ values):

$$\frac{1}{\text{Return period}\ (20\ \text{mm} \cap 300\ \text{Pa})} = \left(1 - \exp^{-\exp^{\frac{16.189 - 18.887}{2.042}}}\right) \cdot \left(1 - \exp^{-\exp^{\frac{12.984 - 8.64}{4.859}}}\right)$$

$$\text{Return period}\ (20\ \text{mm} \cap 300\ \text{Pa}) = 4.7\ \text{years}$$

Based on this result, it seems reasonable to consider a façade

configuration with better performance during the watertightness test, that is capable of withstanding more severe and infrequent atmospheric exposures.

Below, it is determined the pressure difference that a curtain wall configuration should overcome in the EN 12155 trial to achieve 50-year watertightness in the Maastricht case study (26 m height façade surrounded by other tall buildings). For this, Eqs. (2) and (4) define a two-equation system in which the values of the unknowns $U_{10i\ sim}$ and R_{hi} can be solved analytically. As in the previous case, the water supply established in the watertightness test was considered to be WDR exposure (2 mm/min applied over 5 min), and the mode and dispersion parameters were derived from the maximum annual values of wind speed during rainfall. Before solving the equation system, cross-multiplication should be applied, which allows the extrapolation of the hourly values equivalent to those linked with the 5-min duration of the watertightness test:

$$R_{h\ (60\ \mathrm{min})} = R_{h\ (5\ \mathrm{min})} \cdot \frac{9.401 \cdot 60^{-0.804}}{9.401 \cdot 5^{-0.804}} = 0.136 \cdot R_{h\ (5\ \mathrm{min})}$$

$$U_{10\ \mathrm{sim}(60\ \mathrm{min})} = U_{10\ \mathrm{sim}(5\ \mathrm{min})} \cdot \frac{-1.973 \cdot \ln(60) + 21.394}{-1.973 \cdot \ln(5) + 21.394} = 0.731 \cdot U_{10\ \mathrm{sim}(5\ \mathrm{min})}$$

$$R_{h\ (5\ \mathrm{min})} = 0.938\ \mathrm{mm} = 0.188\ \mathrm{mm/min}$$

$$U_{10\ \mathrm{sim}(5\ \mathrm{min})} = 31.750\ \mathrm{m/s}$$

As previously mentioned, the resolution of this equation system also leads to an alternative solution ($R_{hi\ (5min)} = 8.686$ mm and $U_{10i\ sim(5\ min)} = 5.119$ m/s), which is not of interest given that it provides a lower wind speed value (the ΔP value is the key factor for all watertightness tests). Finally, the obtained wind speed enabled the determination of the pressure difference to be surpassed during the watertightness test (Eq. (1)).

$$\mathrm{DRWP} = \Delta P = 1 \cdot \frac{1}{2} \cdot 1.2 \cdot \left(U_{10\mathrm{sim}(5\mathrm{min})}\right)^2 \cdot \left(\frac{26}{10}\right)^{2 \cdot \left[0.18 + 0.13 \cdot \log 3.0 + 0.03 \cdot (\log 3.0)^2\right]} \cdot 1 = 973\ \mathrm{Pa}$$

Although both case studies have been resolved using all available data, the production of additional series of recording intervals is laborious, and in some places, analysing the concurrence between rainfall and wind speed records can become impossible. In the next section, the implementation of the BPB method is exemplified for locations with limited weather records, such as those that are absent from the provided database.

$$10\ mm = 1.14 \cdot 0.9 \cdot \frac{U_{10i\ \mathrm{sim}(5\ \mathrm{min})} \cdot \left(\frac{26}{10}\right)^{\left[0.18 + 0.13 \cdot \log\ 3.0 + 0.03 \cdot (\log\ 3.0)^2\right]}}{-0.16603 \cdot \left(R_{h(5\ \mathrm{min})}\right)^{-1} + 4.92438 \cdot \left(R_{h(5\ \mathrm{min})}\right)^{-0.768} - 0.89002 \cdot \left(R_{h(5\ \mathrm{min})}\right)^{-0.536} + 0.05507 \cdot \left(R_{h(5\ \mathrm{min})}\right)^{-0.304}}$$

$$\frac{1}{50\ \mathrm{years}} = \left(1 - \exp^{-\exp^{\frac{14.639 - \left(0.731 \cdot U_{10i\ \mathrm{sim}(5\ \mathrm{min})}\right)}{2.345}}}\right) \cdot \left(1 - \exp^{-\exp^{\frac{13.767 - \left(0.136 \cdot R_{hi(5\ \mathrm{min})} \cdot 60\right)}{14.586}}}\right)$$

Table 6
Calculation parameters applicable in the two case studies, assuming that only maximum annual records of rainfall and wind speed related to hourly and daily intervals are available.

	AMSTERDAM		
Site conditions:			
Maximum rainfall intensity (mm/min); Average of maximum annual records for both available recording intervals:			
	60' (hour)	**1440' (day)**	Eq. 5
	0.257	0.033	$\Rightarrow R_{h\ (t)} = 3.572 \cdot t^{-0.643}$
$u_{(Rh)}$:	12.984		*(Potential-type regression by LSRA)*
$\beta_{(Rh)}$:	4.859		
Maximum wind speed -without any distinction- (m/s); Average of maximum annual records for both available recording intervals:			
	60' (hour)	**1440' (day)**	Eq. 6
	18.300	13.492	$\Rightarrow U_{10(t)} = -1.513 \cdot \ln(t) + 24.495$
$u_{(u10)}$:	17.000		*(Logarithmic-type regression by LSRA)*
$\beta_{(u10)}$:	2.624		
Extrapolation of conventional extreme values of wind speed U_{10} from those concurrent with rainfall $U_{10\ sim}$ (general linear regression for the Netherlands):			
Eq. 8	$U_{10} = 0.800 \cdot U_{10\ sim} + 5.500$		

	MAASTRICHT		
Site conditions:			
Maximum rainfall intensity (mm/min); Average of maximum annual records for both available recording intervals:			
	60' (hour)	**1440' (day)**	Eq. 5
	0.350	0.027	$\Rightarrow R_{h\ (t)} = 9.3317 \cdot t^{-0.802}$
$u_{(Rh)}$:	13.767		*(Potential-type regression by LSRA)*
$\beta_{(Rh)}$:	14.586		
Maximum wind speed -without any distinction- (m/s); Average of maximum annual records for both available recording intervals:			
	60' (hour)	**1440' (day)**	Eq. 6
	15.800	10.496	$U_{10(t)} = -1.669 \cdot \ln(t) + 22.633$
$u_{(u10)}$:	14.639		*(Logarithmic-type regression by LSRA)*
$\beta_{(u10)}$:	2.345		
Extrapolation of conventional extreme values of wind speed U_{10} from those concurrent with rainfall $U_{10\ sim}$ (general linear regression for the Netherlands):			
Eq. 8	$U_{10} = 0.800 \cdot U_{10\ sim} + 5.500$		

4.2. Implementation of the comprehensive BPB method based on limited weather records

For the purpose of the analysis, only the maximum annual records of rainfall and wind speed related to hourly and daily recording intervals were considered available (i.e., two common recording intervals in multiple locations). These data prevent the production of additional data series related to other recording intervals, as well as obtaining coefficients, mode and dispersion parameters specifically linked to wind records concurrent with rainfall. To simultaneously analyse the sensitivity of the comprehensive BPB method when using limited weather data, the calculation was performed for the same locations and study cases previously addressed, thus allowing validation of the method accuracy compared to the detailed previous calculation. Table 6 presents the data available for the calculation, where only the annual maxima collected from 2010 to 2019 were used.

For the façade in Amsterdam, the wind speed required to produce a DRWP exposure of 300 Pa and the rainfall intensity needed to simultaneously produce a WDR exposure of 2 mm/min over 10 min were the same as those presented in Section 4.1:

$$U_{10(10\ \mathrm{min})} = 22.846\ \mathrm{m/s}$$

$$R_{h\ (10\ \mathrm{min})} = 4.522\ \mathrm{mm} = 0.452\ \mathrm{mm/min}$$

Because the available $u_{(u10)}$ and $\beta_{(u10)}$ values were obtained from the annual maximum values that did not consider concurrency with rainfall, the wind speed obtained using Eq. (1) cannot be directly applied to Eq. (4) (nor in Eq. (6), where the coefficients c and d are derived from the corresponding non-concurrent series of annual maxima, related to hourly and daily intervals). Thus, the general linear regression valid across the Netherlands was used, extrapolating the equivalent value non-concurrent with rainfall (Eq. (8)).

$$U_{10} = 0.800 \cdot 22.846 + 5.500 = 23.777\ \mathrm{m/s}$$

Subsequently, cross-multiplication based on Eqs. (5) and (6) was required to obtain the hourly values corresponding to these 10-min variables:

$$R_{h\ (60\ \mathrm{min})} = R_{h(10\ \mathrm{min})} \cdot \frac{3.572 \cdot 60^{-0.643}}{3.572 \cdot 10^{-0.643}} = 0.143\ \mathrm{mm/min} = 8.57\ \mathrm{mm}$$

$$U_{10(60\ \mathrm{min})} = U_{10(10\ \mathrm{min})} \cdot \frac{-1.513 \cdot \ln(60) + 24.495}{-1.513 \cdot \ln(10) + 24.495} = 20.709\ \mathrm{m/s}$$

The return period associated with the maximum exposure that this façade configuration would withstand at its design operating conditions (Amsterdam, 9 m height, outskirts of the city) can be determined by substituting both hourly values into Eq. (4). As can be seen, the disparity between the results obtained from multiple additional recording intervals and the re-analysis of wind data, barely amounts to 0.4 years (i.e., an 8.51 % difference).

$$\frac{1}{\text{Return period}\ (20\,\mathrm{mm} \cap 300\,\mathrm{Pa})} = \left(1 - \exp^{-\exp^{\frac{17.000 - 20.709}{2.624}}}\right) \cdot \left(1 - \exp^{-\exp^{\frac{12.984 - 8.57}{4.859}}}\right)$$

$$\text{Return period}\ (20\ \mathrm{mm} \cap 300\ \mathrm{Pa}) = 5.1\ \text{years}$$

In the case study by Maastricht, Eq. (8) was added to the system of equations presented in Section 4.1:

$$R_{\mathrm{h}\ (60\ \mathrm{min})} = R_{h\ (5\ \mathrm{min})} \cdot \frac{9.3317 \cdot 60^{-0.802}}{9.3317 \cdot 5^{-0.802}} = 0.136 \cdot R_{h\ (5\ \mathrm{min})}$$

$$U_{10(60\ \mathrm{min})} = \left(0.800 \cdot U_{10\ \mathrm{sim}(5\ \mathrm{min})} + 5.500\right) \cdot \frac{-1.669 \cdot \ln(60) + 22.633}{-1.669 \cdot \ln(5) + 22.633} = 0.634 \cdot U_{10\ \mathrm{sim}(5\ \mathrm{min})} + 4.356$$

$$10\ mm = 1.14 \cdot 0.9 \cdot \frac{U_{10i\ \mathrm{sim}(5\ \mathrm{min})} \cdot \left(\frac{26}{10}\right)^{\left[0.18 + 0.13 \cdot \log 3.0 + 0.03 \cdot (\log 3.0)^2\right]}}{-0.16603 \cdot \left(R_{h(5\ \mathrm{min})}\right)^{-1} + 4.92438 \cdot \left(R_{h(5\ \mathrm{min})}\right)^{-0.768} - 0.89002 \cdot \left(R_{h(5\ \mathrm{min})}\right)^{-0.536} + 0.05507 \cdot \left(R_{h(5\ \mathrm{min})}\right)^{-0.304}}$$

$$\frac{1}{50\ \text{years}} = \left(1 - \exp^{-\exp^{\frac{14.639 - \left(0.634 \cdot U_{10i\ \mathrm{sim}(5\ \mathrm{min})} + 4.356\right)}{2.345}}}\right) \cdot \left(1 - \exp^{-\exp^{\frac{13.767 - \left(0.136 \cdot R_{hi(5\ \mathrm{min})} \cdot 60\right)}{14.586}}}\right)$$

$$R_{h\ (5\ \mathrm{min})} = 1.020\ \mathrm{mm} = 0.204\ \mathrm{mm/min}$$

$$U_{10\ \mathrm{sim}(5\ \mathrm{min})} = 29.667\ \mathrm{m/s}$$

The alternative solution ($R_{hi\ (5min)} = 8.643$ mm and $U_{10i\ sim\ (5\ min)} = 5.140$ m/s) was not of interest because it provided a lower wind speed value. Finally, the pressure difference to be surpassed during the EN 12155 watertightness test was calculated using Eq. (1). In this case, there was a pressure difference of 125 Pa compared to the result obtained in Section 4.1 (with a percentage difference of 12.82 %).

$$DRWP = \Delta P = 1 \cdot \frac{1}{2} \cdot 1.2 \cdot \left(U_{10\mathrm{sim}(5\mathrm{min})}\right)^2 \cdot \left(\frac{26}{10}\right)^{2 \cdot \left[0.18 + 0.13 \cdot \log 3.0 + 0.03 \cdot (\log 3.0)^2\right]} \cdot 1 = 850\mathrm{Pa}$$

The proposed implementation maintained reasonable accuracy in both case studies (percentage differences below 13 %; 8.5 % for the façade in Amsterdam and 12.6 % in the case study by Maastricht), even though the concurrent occurrence of wind speed and rainfall records was not analysed and a generic linear regression valid across the entire country was used. Therefore, applying Eq. (8) is possible owing to the homogeneous characteristics of the Netherlands. Future studies should analyse the validity of such generalisations in other regions with greater topographic and climatic variations and establish regional variations if necessary (Eqs. (5) and (6) were extensively validated in this regard [46]).

If both analyses are repeated omitting Eq. (8) (i.e., using limited climatic data and directly applying the wind speed obtained using Eq. (1) to Eq. (4)), the result would be a return period of 3.9 years for the façade in Amsterdam (the error increases up to 17.0 % regarding section 4.1) and a pressure difference of 824 Pa in the Maastricht case study (error equal to 15.3 %). These results demonstrate the usefulness of both proposed methodological improvements, not only enabling the analysis in locations with limited climatic records but also considering the local or regional concurrence of extreme wind records with rainfall.

The increasing implementation of automatic weather stations and greater accessibility to exhaustive climate data should enable the expansion of the provided database in the future, considering a larger number of locations and recording intervals that align more closely with the duration of the pressure stages used in the watertightness tests. This would further reduce the uncertainty of extrapolations in the BPB method (Eqs. (5) and (6)) and allows the analysis of concurrence

between wind speed data series and rainfall at each site (Eq. (7)), thus enabling the comprehensive implementation of the BPB method everywhere. In any case, it is important to remember that the performance-based design of building façades to resist rainwater penetration should not disregard the application of safety factors, advisable by the stochastic nature of both variables analysed (specially in a context of changing climate) and due to the hypothetical deviations resulting from the availability of limited weather data.

5. Conclusions

In this study, new contributions were developed to enhance a procedure (the BPB method) that quantitatively relates WDR and DRWP exposures on building façades with the results of standardised watertightness tests, thus allowing a performance-based design of façades against rainwater penetration. General forms of regression equations that relate extreme values of rainfall and wind speed across sub-daily intervals and a functional extrapolation of extreme wind speeds based on wind records concurrent with rainfall were included in the calculation. As a result, the reliability of the method is improved by effectively considering the co-occurrence of rainfall and wind speed when calculating return periods, while computational effort and reliance on exhaustive weather records are reduced.

The functional implementation of this perfected BPB method in two hypothetical case studies (façades located in Amsterdam and Maastricht) demonstrated its ability to avoid qualitative and poorly optimised practitioner decisions. The results obtained suggest that an accurate characterisation of façade watertigthness performance is also possible, even based on the maximum annual summaries of rainfall and wind speed linked to hourly and daily recording intervals (differences of less than 13 % regarding the results based on exhaustive data were identified). Incorporating the comprehensive BPB method into building codes (by simply establishing the required watertightness performance, i.e., fixing the return period) represents a step forward in addressing the current lack of correlation between the practitioner's façade designs and the actual WDR and DRWP exposures on them. Finally, a comprehensive dataset of calculation parameters was provided to enable façade performance-based designs throughout the Netherlands.

CRediT authorship contribution statement

José M. Pérez-Bella: Writing – original draft, Funding acquisition, Conceptualization. **Javier Domínguez-Hernández:** Writing – review & editing, Funding acquisition, Formal analysis. **Pedro L. López-Julián:** Methodology, Investigation, Formal analysis. **Ángel Salesa-Bordabana:** Validation, Software, Data curation. **Martín Orna-Carmona:** Visualization, Supervision, Resources.

Declaration of Generative AI and AI-assisted technologies in the writing process

During the preparation of this work the authors did not use Generative AI. The authors reviewed and edited the content as needed and take full responsibility for the content of the publication. Readability and language was improved by Elsevier Language Editing Services.

Declaration of competing interest

We wish to confirm that there are no known conflicts of interest associated with this manuscript and there has been no significant financial support for this work that could have influenced its outcome.

All the supports have been mentioned in the Acknowledgements section: *Project PID2021-122203OB-I00 funded by MCIN/AEI/10.13039/501100011033 and by ERDF A way of making Europe. These results have been obtained from weather data provided by The Royal Netherlands Meteorological Institute (KNMI). The authors acknowledge engineer Ricardo Fañanás Maza his help in the data processing as well as the collaboration of doctor in industrial engineering Elena Ibarz Montaner.*

We confirm that we have given due consideration to the protection of intellectual property associated with this work and that there are no impediments to publication with respect to intellectual property. In so doing we confirm that we have followed the regulations of our institutions concerning intellectual property.

This manuscript has not been submitted for publication nor has it been published in whole or in part elsewhere. In turn, this research paper has not been previously published, is not currently submitted for review to any other journal, and will not be submitted elsewhere during peer review for publication in *Building and Environment*.

Data availability

We have shared the database as supplementary material.

Acknowledgements

Project *PID2021-122203OB-I00* funded by MCIN/AEI/10.13039/501100011033 and by ERDF A way of making Europe. These results have been obtained from weather data provided by The Royal Netherlands Meteorological Institute (KNMI). The authors acknowledge engineer Ricardo Fañanás Maza his help in the data processing as well as the collaboration of doctor in industrial engineering Elena Ibarz Montaner.

Appendix A. Supplementary data

Supplementary data to this article can be found online at https://doi.org/10.1016/j.buildenv.2023.111083.

References

[1] P. Gholamalipour, H. Ge, T. Stathopoulos, Wind-driven rain (WDR) loading on building facades: a state-of-the-art review, Build. Environ. 221 (2022), 109314, https://doi.org/10.1016/j.buildenv.2022.109314.
[2] T. Qian, H. Zhang, Assessment of long-term and extreme exposure to wind-driven rain for buildings in various regions of China, Build. Environ. 189 (2021), 107524, https://doi.org/10.1016/j.buildenv.2020.107524.
[3] B. Blocken, J. Derome, J. Carmeliet, Rainwater runoff from building façades: a review, Build. Environ. 60 (2013) 339–361, https://doi.org/10.1016/j.buildenv.2012.10.008.
[4] S. Van Kinden, N. Van den Bossche, Review of rainwater infiltration rates in wall assemblies, Build. Environ. 219 (2022), 109213, https://doi.org/10.1016/j.buildenv.2022.109213.
[5] E.A. Støver, M.H. Sundsøy, E. Andenæs, S. Geving, T. Kvande, Rain intrusion through horizontal joints in façade panel systems - experimental investigation, Buildings 12 (2022) 1497, https://doi.org/10.3390/buildings12101497.
[6] S. Kahangi, J. Niklewski, M. Molnár, Experimental investigation of water absorption and penetration in clay brick masonry under simulated uniform water spray exposure, J. Build. Eng. 43 (2021), 102583, https://doi.org/10.1016/j.jobe.2021.102583.
[7] L. Olsson, Driving Rain Tightness, Intrusion Rates and Phenomenology of Leakages in Defects of Façades: A New Calculation Algorithm, Chalmers University of Technology, Gothenburg, 2018. PhD Thesis.
[8] M. Arce, S. García, N. Van den Bossche, Experimental assessment of rainwater management of a ventilated façade, J. Build. Phys. 42 (1) (2017) 38–67, https://doi.org/10.1177/1744259117719077.
[9] S. Yu, X. Liu, Y. Li, S. He, Y. Yao, S. Sun, Experimental and numerical simulation study on hygrothermal migration of damaged envelope walls during wind-driven rain, Build, Environ. Times 243 (2023), 110653, https://doi.org/10.1016/j.buildenv.2023.110653.
[10] A. Erkal, D. D'Ayala, L. Sequeira, Assessment of wind-driven rain impact, related surface erosion and surface strength reduction of historic building materials, Build. Environ. 57 (2012) 336–348, https://doi.org/10.1016/j.buildenv.2012.05.004.
[11] S.A. Orr, M. Cassar, Exposure indices of extreme wind-driven rain events for built heritage, Atmosphere-Basel 11 (2020) 163, https://doi.org/10.3390/atmos11020163.
[12] M.J. Mendell, A.G. Mirer, K. Cheung, M. Tong, J. Douwes, Respiratory and allergic health effects of dampness, mold, and dampness-related agents: a review of the epidemiologic evidence, Environ. Health Perspect. 119 (2011) 748–756, https://doi.org/10.1289/ehp.1002410.
[13] T.A. Pakkala, A. Köliö, J. Lahdensivu, M. Kiviste, Durability demands related to frost attack for Finnish concrete buildings in changing climate, Build. Environ. 82 (2014) 27–41, https://doi.org/10.1016/j.buildenv.2014.07.028.

[14] T.A. Pakkala, J. Lahdensivu, P. Huuhka, H. Kivioja, A.M. Lemberg, Freeze-thaw damage dependence on wind-driven rain of outdoor exposed concrete – a case study, Nord. Concr. Res. 61 (2) (2019) 91–106, https://doi.org/10.2478/ncr-2019-0010.
[15] S.A. Orr, H. Viles, Characterisation of building exposure to wind-driven rain in the UK and evaluation of current standards, J. Wind Eng. Ind. Aerod. 180 (2018) 88–97, https://doi.org/10.1016/j.jweia.2018.07.013.
[16] P. Narula, K. Sarkar, S. Azad, Indexing of driving rain exposure in India based on daily gridded data, J. Wind Eng. Ind. Aerod. 175 (2018) 244–255, https://doi.org/10.1016/j.jweia.2018.02.003.
[17] CEN, EN ISO 15927-3, Hygrothermal Performance of Buildings - Calculation and Presentation of Climatic Data Part 3: Calculation of a Driving Rain Index for Vertical Surfaces from Hourly Wind and Rain Data, European Committee for Standardization, Brussels, 2009.
[18] V.M. Nik, S.O. Mundt-Petersen, A. Sasic, P. de Wilde, Future moisture loads for building facades in Sweden: climate change and wind-driven rain, Build. Environ. 93 (2015) 362–375, https://doi.org/10.1016/j.buildenv.2015.07.012.
[19] S. Kim, D. Zikelbach, H.M. Künzel, Wind-driven rain exposure on building envelopes taking into account frequency distribution and correlation with different wall orientations, Build, Environ. Times 209 (2022), 108665, https://doi.org/10.1016/j.buildenv.2021.108665.
[20] Z. Xiao, M.A. Lacasse, E. Dragomirescu, M. Defo, Projected changes of wind-driven rain and moisture load in wall assemblies across Canada, J. Wind Wng. Ind. Aerod. 238 (2023), 105446, https://doi.org/10.1016/j.jweia.2023.105446.
[21] J.M. Pérez, J. Domínguez, J.J. del Coz, J.E. Martínez, Directional characterisation of annual and temporary exposure to rainwater penetration on building façades throughout Mexico, Build. Environ. 212 (2022), 108837, https://doi.org/10.1016/j.buildenv.2022.108837.
[22] J. Domínguez, J.M. Pérez, M. Alonso, E. Cano, J.J. del Coz, Assessment of water penetration risk in building façades throughout Brazil, Build. Res. Inf. 45 (5) (2016) 1–16, https://doi.org/10.1080/09613218.2016.1183441.
[23] J.M. Pérez, J. Domínguez, E. Cano, J.E. Martínez, J.J. del Coz, Avoiding the need to directionally determine the exposure to rainwater penetration for façade designs, Build. Environ. 176 (2020), 106850, https://doi.org/10.1016/j.buildenv.2020.106850.
[24] J.M. Pérez, J. Domínguez, E. Cano, J.J. del Coz, F.P. Álvarez Rabanal, On the significance of the climate-dataset time resolution in characterising wind-driven rain and simultaneous wind pressure. Part II: directional analysis, Stoch. Environ. Res. Risk Assess. 32 (2018) 1799–1815, https://doi.org/10.1007/s00477-017-1480-2.
[25] L. Shi, L. Tao, Y. Zhang, Y. Li, X. Jiang, Z. Yang, X. Qi, J. Qiu, CFD simulations of wind-driven rain on typical football stadium configurations in China's hot-summer and cold-winter zone, Build, Environ. Times 225 (2022), 109598, https://doi.org/10.1016/j.buildenv.2022.109598.
[26] X. Zhou, A. Kubilay, D. Derome, J. Carmeliet, Comparison of wind-driven rain load on building facades in the urban environment and open field: a case study on two buildings in Zurich, Switzerland, Build, Environ. Times 233 (2023), 110038, https://doi.org/10.1016/j.buildenv.2023.110038.
[27] CEN, EN ISO 12865, Hygrothermal Performance of Building Components and Building Elements - Determination of the Resistance of External Wall Systems to Driving Rain under Pulsating Air Pressure, European Committee for Standardization, Brussels, 2001.
[28] AS/NZS 4284, Testing of Building Façades, Australian/New Zealand Standards, Sydney/Wellington, 2008.
[29] ASTM International, ASTM E514, Standard Test Method for Water Penetration and Leakage through Masonry, American Society for Testing and Materials, West Conshohocken, 2020, https://doi.org/10.1520/E0514_E0514M-20.
[30] ASTM International, ASTM E547, Standard Test Method for Water Penetration of Exterior Windows, Skylights, Doors, and Curtain Walls by Cyclic Static Air Pressure Difference, American Society for Testing and Materials, West Conshohocken, 2016, https://doi.org/10.1520/E0547-00R16.
[31] Singapore Standards Council, SS 654, Code of Practice for Curtain Walls, Enterprise Singapore, Singapore, 2020.
[32] J.M. Pérez, J. Domínguez, B. Rodríguez, J.J. del Coz, E. Cano, A new method for determining the water tightness of building facades, Build. Res. Inf. 41 (4) (2013) 401–414, https://doi.org/10.1080/09613218.2012.774936.
[33] J.M. Pérez, J. Domínguez, B. Rodríguez, J.J. del Coz, E. Cano, A. Navarro, An extended method for comparing watertightness tests for facades, Build. Res. Inf. 41 (6) (2013) 706–721, https://doi.org/10.1080/09613218.2013.823538.
[34] J.M. Pérez, J. Domínguez, B. Rodríguez, E. Cano, J.J. del Coz, F.P. Álvarez, Improvement alternatives for determining the watertightness performance of building facades, Build. Res. Inf. 43 (6) (2015) 723–736, https://doi.org/10.1080/09613218.2014.943101.
[35] S.M. Cornick, M.A. Lacasse, A review of climate loads relevant to assessing the watertightness performance of walls, windows and wall-window interfaces, J. ASTM Int. (JAI) 2–10 (2005) 1–15, https://doi.org/10.1520/JAI12505.
[36] F. Bañuelos, C. Ángeles, S. Ríos, Analysis and validation of the methodology used in the extrapolation of wind speed data at different heights, Renew. Sustain. Energy Rev. 14 (2010) 2383–2391, https://doi.org/10.1016/j.rser.2010.05.001.
[37] A.S. Smedman-Högström, U. Högström, A practical method for determining wind frequency distributions for the lowest 200 m from routine meteorological data, J. Appl. Meteorol. 17 (1978) 942–954, 0021-8952/0942-0954$06.50.
[38] G. Gualteri, S. Secci, Comparing methods to calculate atmospheric stability-dependent wind speed profiles: a case study on coastal location, Renew. Energy 36 (2011) 2189–2204, https://doi.org/10.1016/j.renene.2011.01.023.
[39] M.Z. Jacobson, Fundamentals of Atmospheric Modelling, second ed., Cambridge University Press, New York, 2005.
[40] WMO, Guide to Meteorological Instruments and Methods of Observation (WMO No. 8), World Meteorological Organisation, Geneva, 2008.
[41] J.F. Straube, E.F.P. Burnett, Simplified prediction of driving rain on buildings, in: Proceedings International Building Physics Conference, 2000, pp. 375–382. Eindhoven.
[42] N. Van denr Bossche, M.A. Lacasse, A. Janssens, A uniform methodology to establish test parameters for watertightness testing part II: pareto front analysis on co-occurring rain and wind, Build. Environ. 63 (2013) 157–167, https://doi.org/10.1016/j.buildenv.2012.12.019.
[43] A.N. Dingle, W. Lee, Terminal fall speeds of raindrops, J. Appl. Meteorol. 11 (1972) 877–879, https://doi.org/10.1175/1520-0450(1972)011<0877:TFOR>2.0.CO;2.
[44] S.M. Cornick, A. Dalgliesh, N. Said, R. Djebbar, F. Tariku, M.K. Kumaran, Report from Task 4 of MEWS Project: Task 4 – Environmental Conditions Final Report (Research Report No. 113), National Research Council Canada, Ottawa, 2002.
[45] A. Hansen, The three extreme value distributions: an introductory review, Front. Physiol. 8 (2020), 604053, https://doi.org/10.3389/fphy.2020.604053.
[46] J.M. Pérez, J. domínguez, J.E. Martínez, M. Alonso, J.J. del Coz, An alternative approach to estimate any subdaily extreme of rainfall and wind from usually available records, Stoch, Environ. Res. Risk Assess. 36 (2022) 1819–1833, https://doi.org/10.1007/s00477-021-02144-4.
[47] G. Kemmer, S. Keller, Nonlinear least-squares data fitting in Excel spreadsheets, Nat. Protoc. 5 (2010) 267–281, https://doi.org/10.1038/nprot.2009.182.
[48] Royal Netherlands Meteorological Institute (KNMI), Weather Stations – Hourly Records, 2023 (in Dutch), https://www.daggegevens.knmi.nl/klimatologie/uurgegevens. (Accessed 27 July 2023).
[49] M.C. Peel, B.L. Finlayson, T.A. Mcmahon, Updated world map of the Köppen-Geiger climate classification, Hydrol. Earth Syst. Sci. 11 (2007) 1633–1644, https://doi.org/10.5194/hess-11-1633-2007.
[50] M.C. Serreze, F. Carse, R.G. Barry, J.C. Rogers, Icelandic Low cyclone activity: climatological features, linkages with the NAO, and relationships with recent changes in the Northern hemisphere circulation, J. Clim. 10–3 (1997) 453–464, https://doi.org/10.1175/1520-0442(1997)010%3c0453:ILCACF%3e2.0.CO;2.
[51] CEN, EN 12154, Curtain Walling - Watertightness - Performance Requirements and Classification, European Committee for Standardization, Brussels, 1999.
[52] CEN, EN 12155, Curtain Walling - Watertightness - Laboratory Test under Static Pressure, European Committee for Standardization, Brussels, 2000.